CrystEngComm

Accepted Manuscript

This is an *Accepted Manuscript*, which has been through the Royal Society of Chemistry peer review process and has been accepted for publication.

Accepted Manuscripts are published online shortly after acceptance, before technical editing, formatting and proof reading. Using this free service, authors can make their results available to the community, in citable form, before we publish the edited article. We will replace this *Accepted Manuscript* with the edited and formatted *Advance Article* as soon as it is available.

You can find more information about *Accepted Manuscripts* in the Information for Authors.

Please note that technical editing may introduce minor changes to the text and/or graphics, which may alter content. The journal's standard Terms & Conditions and the Ethical guidelines still apply. In no event shall the Royal Society of Chemistry be held responsible for any errors or omissions in this *Accepted Manuscript* or any consequences arising from the use of any information it contains.

ROYAL SOCIETY OF CHEMISTRY

www.rsc.org/crystengcomm

CrystEngComm

RSCPublishing

Paper

Optimizing Packing Density of TiO_2 Nanorod Array for Enhanced Light Harvesting by Light Trapping Effect and Its Photocatalytic Decomposition of Gaseous Benzene

Cite this: DOI: 10.1039/xoxxooooox

Received ooth January 2012,
Accepted ooth January 2012

DOI: 10.1039/xoxxooooox

www.rsc.org/

Xiaoxia Wang,[a] Yadan Xiao,[b] Dawen Zeng[ab] and Changsheng Xie[b]

As photocatalysts, semiconductors can demonstrate a novel performance when the morphology is appropriately manipulated. In this paper, single-crystalline TiO_2 nanorod array with a preferred [002] axial orientation was grown on transparent conductive fluorine-doped tin oxide (FTO) substrates by a hydrothermal process. The packing density of the nanorod array was manipulated by simply changing the hydrochloride acid (HCl) / water volume ratio of the initial growth solution. The growth mechanism of the nanorod array was discussed. Measurements of XRD, SEM and TEM suggest that more (002) facets were exposed on top of the nanorod with a higher packing density. However, the array with most (002) facets exposed demonstrates relatively low photocatalytic activity targeting gaseous benzene. Results indicate that the nanorod array is better compiled with a medium packing density (46.6%) to double the photocatalytic performance comparing to both 15.26% and 81.25% packed arrays. The UV-Vis absorption measurement and photocurrent test reveal that a medium packing density can provide a greatly enhanced light harvesting efficiency due to light trapping effect by the array structure. By establishing a simple-but-efficient leverage to manipulate the packing density of the nanorod film, the photocatalytic activity of the array is greatly impacted by variation of light harvesting efficiency due to light trapping effect rather than more exposed high energy facets.

Introduction

Nowadays, air pollution has become a severe problem in our daily life. And among them, volatile organic compound (VOC) is a rising one for indoor pollution.[1-3] As we known, VOCs drew a lot of attention due to its harmfulness to human health, causing headache, coughing, and cancer.[4] Typical VOC such as benzene is widely used in industry, like furniture manufacturing, building materials or paints, then the benzene would gradually release during time,[3,5] which is inhaled by human, causing health problems.

As we know, since the photocatalytic activity of TiO_2 was discovered, photocatalytic nanomaterials have been considered as an ideal leverage to solve the VOCs pollution.[6,7] One of the unique features of photocatalytic nanomaterials is that it can utilize the light source to break the contaminants into small molecules such carbon dioxide and water,[8] which is unharmful to human health. However, there are still some bottlenecks that restrict the practical application of photocatalysts, such as how to load them to the surface of substrates.[9,10] As for photocatalysts in powder form loaded on the surface of substrates, they often easily peel off due to the poor adhesion. When powder photocatalysts are mixed into substrates like paint, for example, it will be hard for photocatalysts to engage pollutants for photo-degradation. Fortunately, synthesized by using FTO glass as templates, a vertically oriented rutile TiO_2 nanorod array demonstrates great adhesion between TiO_2 and the glass substrate and it exhibits potential for further manipulation and decoration.[11]

Compared to the early TiO_2 nanorod arrays were fabricated with presence of multifarious chemicals by cumbersome steps, using FTO as templates by hydrothermal method has advantages of one-step convenience and extremely low-cost.[12-14] Moreover, this self-assembled and vertically oriented rutile TiO_2 nanorod array has unique uniformed structure, which is suitable for further morphology adjustment.[15,16] But most importantly, the nanorod array can provide un-interrupted electrical pathways for photogenerated charge carriers along the grown axis of [002] direction due to its single-crystalline property[15,16]. And the nanorod has (002) facets exposed on top. Interestingly, these two properties mentioned above are crucial for photocatalysts.[8,17] On account of the nanorod's single-crystalline structure, photo-generated electrons can easily transferred to the conductive side of FTO with less recombination to holes on grain boundaries, which prolongs the lifetime of photo-generated electrons and holes, providing more valid charge carriers for photocatalysis.[18] Based on many researches, the (002) facets of TiO_2 are generally considered as high energy facets, which is benefit for higher photocatalytic activity. Another advantage of the nanorod array is that the structure of the array is facile to be manipulated and for further decorations. Based on Liu's work, Zhang successfully achieved structural engineering of the nanorod array by substituting ethanol for water as a solvent, monitoring the [002] directional growth as well as the packing density of the array.[19] Moreover, Huang successfully established a controllable synthesis method of nanorod array with different packing density as well as various diameters, which is achieved by adding glacial acetic acid to control the hydrolysis of titanium precursor and the growth of the nanorods.[20] Both of Zhang and Huang's work are focused on controlling the hydrolysis rate of titanium precursor to fabricate nanorod arrays with different morpholo-

CrystEngComm Accepted Manuscript

gy. However, the impact of the nanorod array's morphology or the exposed high energy (002) facets to the photocatalytic performance is still uninvestigated.

In this paper, we successfully introduced a more facile hydrothermal method to synthesize rutile TiO_2 nanorod array with different packing density, by simply changing the HCl/water ratio of ingredients to control the hydrolysis rate of titanium butoxide. The result shows that a nanorod array with largely (002) facets exposed can be obtained along with higher packing density. However, the nanorod array with most (002) facets exposed didn't exhibit the best photocatalytic performance targeting gaseous benzene. Results indicated that an appropriate packing density can provide ideal architecture for light trapping effect, which promotes the photocatalytic performance. This gives us rethinks that for materials with uniformed structure, the light absorbance ability due to structure characteristics is a nonnegligible factor to consider.

Materials and methods

Reagents

All the chemicals used in this study were analytical grade and used without further purification. Distilled water was used in all experiments. Ethanol, hydrochloric acid, and titanium butoxide (TnBT) were bought from Sinopharm Chemical Reagent Co., Ltd. The FTO coated glass (F:SnO_2, 14Ω/square) was bought from NSG group of Japan.

Synthesis of TiO_2 nanorod array

TiO_2 nanorod arrays were successfully achieved by a modified hydrothermal method based on the previous work of Liu and Aydil.[11] The synthesis procedure began with the cleaning of FTO coated glass. The substrates were ultrasonically cleaned for 60 min in a mixed solution of distilled water, acetone and 2-propanol with volume ratios of 1:1:1, followed by drying in ambient condition. 24 mL of distilled water was mixed with 24 mL of concentrated hydrochloric acid (36.5%- 38% by weight) to reach a total volume of 48 mL in a Teflon-lined stainless steel autoclave (100 mL volume). To achieve different packing density, we changed the hydrochloric acid usage in the range from 12 to 26 mL by intervals of 2 mL, while keeping the solution's total volume at 48 mL. The sample using 12 mL HCl in the synthesis was labeled as S12 and the rest samples were labeled by this analogy as well.The formula was plotted as Table 1 shows. The mixture was stirred at ambient conditions for 5 min before the addition of 0.5 mL of titanium butoxide. After stirring for another 5 min, a piece of pre-cleaned FTO glass (50 mm×25 mm) was placed at an angle against the wall of Teflon-liner with the conducting side facing down. The hydrothermal process was conducted under 150℃ for 20 h in an electric oven. After synthesis, the autoclave was cooled to temperature under flowing water, which took approximately 15 min. The substrate was taken out and rinsed extensively by massive amount of distilled water. The packing density of the TiO_2 array was manipulated by changing the volume ratio of hydrochloric acid and distilled water in the hydrothermal process.

Table 1 Ingredients of the growth solution for different samples

Sample Label	HCl (mL)	H_2O (mL)	TnBT (mL)
S12	12	16	0.5
S14	14	34	0.5
S16	16	32	0.5
S18	18	30	0.5
S20	20	28	0.5
S22	22	26	0.5
S24	24	24	0.5
S26	26	22	0.5

Characterization

The planar and cross-sectional morphology of the TiO_2 nanorod thin films were observed by field-emission scanning electron microscopy (FESEM, FEI Sirion 200), which was operated at an acceleration voltage of 10 kV. Transmission electron microscope (TEM) measurements were carried out with a FEI Tecnai G2 S-TWIM working at 200 kV. The X-ray diffraction (XRD) patterns were recorded by a Philips X'Pert diffractometer from 2θ = 20°to 80°using Cu-Kα radiation (λ = 1.5406 Å). UV-Vis absorption spectra were recorded using PerkinElmer Lambda 35 UV-Vis diffuse reflectance spectrometer; $BaSO_4$ was used as reference. The photoelectric properties of TiO_2 films were measured by a test platform developed by our laboratory.[21] The whole test process was carried out under a dry air stream at room temperature with a bias for 3 volts, and the flow of air stream was controlled as 200 mL/min. An ultraviolet (UV) LED array light (Light Emitting Diode, Shenzhen Ti-Times Co.) was used for illuminating the samples as the excitation source. The wavelength of the UV light was 365 nm and the illumination intensity was 36 W/m^2. In order to get a steady photocurrent-time curve, a test mode whose UV illumination was turned on at 300 s and off at 600 s was used, and the whole test process was finished at 900 s.

Photocatalytic measurement

Photocatalytic performance of the samples was evaluated by degrading gaseous benzene under irradiation of UV light at ambient temperature in a 2 L cubic reactor, before which the air tightness of the reactor was tested. The UV light was generated from a Xenon lamp (UV300, Aulight of China Co., LTD) with a wavelength range of 200 - 400 nm. After two pieces of the FTO substrates with TiO_2 thin films on them were placed into the reactor, aqueous benzene with a volume of 1 μL was also injected within by a syringe. The bottom of the reactor was slightly heated (below 40℃) to ensure benzene all evaporated. Reactor was kept as is till reaching an adsorption-desorption equilibrium before the irradiation of UV light. The analysis of the concentration of benzene and CO_2 was performed with a gas chromatography (GC9560, Shanghai Huaai Co., LTD). Each set of experiments was monitored for 3 h.

Results and discussion

Effect of growth solution's PH on the structure of the array

Generally, nanorod films were successfully grown on the FTO substrates at 150℃ for 20 h. But for the sets of experiments by using 12 mL and 26 mL HCl, no nanorod has been found on the FTO substrates after the hydrothermal process. Fig. 1 displays the planar and cross-section view of the nanorod array. Being consistent with the work of Liu and Aydil,[11] the films are made of vertically oriented nanorods, together with some misoriented rods. For all the samples, the length of the rods is approximately 2 μm. But samples with less HCl usage have a slightly thick-

CrystEngComm Accepted Manuscript

This journal is © The Royal Society of Chemistry 2012

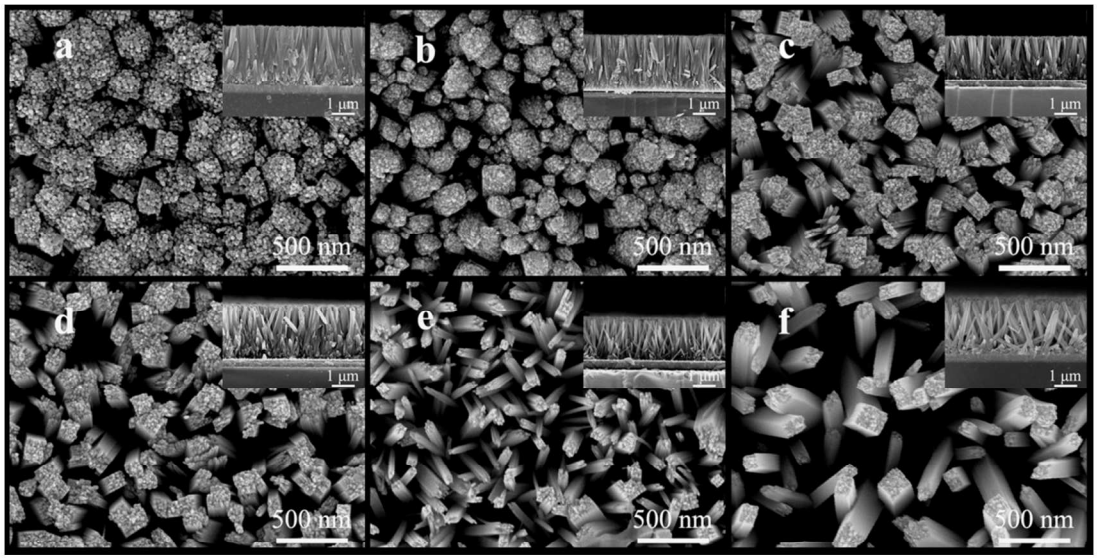

Fig. 1 SEM images of the planar morphology and cross-section view of the nanorod films of sample (a) S14, (b) S16, (c) S18, (d) S20, (e) S22 and (f) S24.

er film due to less-suppressed hydrolysis of TnBT, which could provide more growing units, such as S14.[11] Each single nanorod is a bundle of densely packed nanofibers. As shown in the SEM images, density of the nanorods gradually become looser by increasing the HCl usage and the nanorods tend to be not as vertical as the rods in Fig. 1a.

XRD shows that the films deposited on the FTO substrates are rutile TiO_2. Fig. 2 displays the XRD patterns of the samples. All the diffraction peaks that appeared agree with the tetragonal rutile TiO_2 (SG, $P4_2/mnm$; JCPDS No.88 — 1175, a = b = 0.4517 nm and c = 0.2940 nm). Corresponding to the work of Liu and Zhang, only (101) and (002) peaks can be seen from the spectra.[11,19,20] Moreover, the (002) peak is significantly enhanced, which means the growth of the nanorod is highly oriented. Absence of the other diffraction peaks that are normally present in polycrystalline samples strongly indicate that nanorod is probably single crystalline through their length. It is worth noticing that as well as the density of the nanorods, the intensity of (002) peak also increases while the HCl usage decreases. To verify our speculation, the nanorod was observed by TEM.

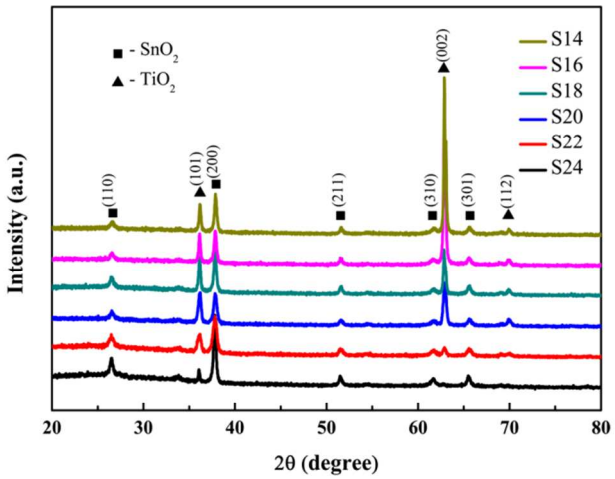

Fig. 2 XRD spectra of the samples fabricated with different HCl usage.

HRTEM confirms that the TiO_2 film is formed by single crystalline nanorods, as evidenced by the sharp SAED pattern in Fig. 3 Each nanorod is comprised of nanofibers with the diameter around 5 nm. The interplanar spacing of (110) is 3.2 Å, which is consistent with rutile phase. The nanorods grow along

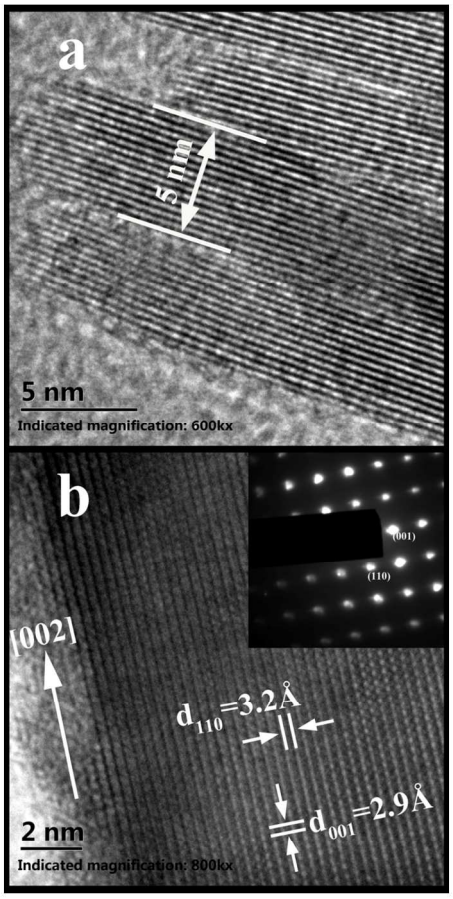

Fig. 3 (a) HRTEM image of the nanorod. (b) the SAED pattern of the single crystalline nanorod.

CrystEngComm Accepted Manuscript

the [002] direction. This explains the greatly enhanced intensity of (002) peak in the result of XRD.

It is well-accepted that there are two key steps during the synthesis to influence the morphology of the nanorod film.[13,19] The first step is the hydrolysis of titanium butoxide when it is being added. The second step is the condensation process which is for the heterogeneous nucleation and growth of TiO_2 nanorods on the FTO substrates. Based on kinetics of nucleation and growth, the nucleation and growth speed of TiO_2 can be promoted by providing more titanium precursors, which is proportional to the hydrolysis speed of titanium butoxide. However, the hydrolysis speed of titanium butoxide is manipulated by using different amount of HCl, playing as a suppressor for the hydrolysis process. Less dose of the HCl, higher the hydrolysis speed is, yielding more TiO_2 growing units (e.g., $[Ti(OH)_2Cl_2(OH)_2]^0$) for nucleation, which leads to a higher nucleation rate of TiO_2.[11] Low nucleation rate leads to uncompetitive growing, consequently the nanorods could randomly grow in different directions. On the contrary, high nucleation rate leads to a dense distribution of the seeds, leaving no space for random growth but vertical growth. Hence, the samples using less HCl have a larger packing density, and the nanorods tend to be more vertically aligned. As for the sample S12, because the hydrolysis of titanium butoxide is not adequately suppressed, it causes a rapid hydrolysis. With a relatively high concentration of titanium precursor, it is more likely to homogeneously precipitate rather than heterogeneously nucleate on the FTO substrates. For this reason, no nanorod was found on the FTO substrates for the sample S12. For the situation of S26, the hydrolysis stage is totally suppressed, so there is barely titanium precursor to meet the requirement of nucleation. Therefore, no nanorod was found as well. Compared to the methods of Zhang and Huang, we also successfully monitored the morphology of the nanorod array by controlling the hydrolysis rate of the titanium precursor but in a more facile way.[19,20]

For quantization of the film's packing density, we calculated the area in each SEM photo (the planar view, single photo covers area of 4608506 nm^2) that the nanorods cover. We counted 5 photos of each sample and average the value in order to be more accurate. The results are listed in Table 2, in which we also listed the proportion of the peak intensity between (002) and (101) from the XRD spectra ($I_{peak(002)}/I_{peak(101)}$). From the table, it's obvious that the percentage of the nanorods' area demonstrates a similar trend as the $I_{peak(002)}/I_{peak(101)}$. Analysis of XRD and TEM indicates that the nanorods are highly ordered single-crystalline nanorod with (002) facets exposed on top. Therefore it's no wonder the value of $I_{peak(002)}/I_{peak(101)}$ increases as the packing density does. And this is another proof for single-crystalline of the nanorods. Since the statistic property of XRD, we scaled the packing density of the films by using the proportion of $I_{peak(002)}/I_{peak(101)}$.

Table 2 The packing density of the samples with different HCl usage

Sample	The area of the nanorods (nm^2)	The percentage of the nanorods' area (%)	$I_{peak(002)} / I_{peak(101)}$
S14	3744453	81.25	5.96
S16	3099852	67.26	2.66
S18	2333831	50.64	1.25
S20	2147633	46.60	1.38
S22	794541	17.24	0.39
S24	703254	15.26	0.10

Photocatalytic activity of the nanorod array

To our best knowledge, (001) facet of rutile TiO_2 is considered as a more reactive facet than other facets due to its low oxygen vacancy formation energy on the facet and it plays an important role by not hindering the removals of the products formed during photocatalysis at the first monolayer, which is a major problem for other surfaces.[22,23] Recently, many researches indicate TiO_2 materials with exposed (001) facet manifested enhanced physicochemical properties in photocatalysis.[24,25] Hence, it's worth measuring the photocatalytic activity of the samples and the results are shown in Fig. 4. However, the photocatalytic performance of the samples didn't demonstrate a linear variation as the packing density does. Nanorod array with too large or too low packing density both showed inhibited photocatalytic performance. Judged by our results, 20 mL is the optimum volume of HCl to use in the synthesis procedure to fabricate TiO_2 nanorod films with the best photocatalytic performance. It decomposed nearly 66% of the benzene in 3 h compared to 44% that sample S24 did, and it generated twice the carbon dioxide as much as the sample S24 did also. Sample S14 presented basically the same photocatalytic activity as sample S24 did.

Fig. 5 lays out the total CO_2 generated during the photocatalytic test and the ratio of peak intensity between (002) and (101) peaks of every sample. The proportion of (002) facets

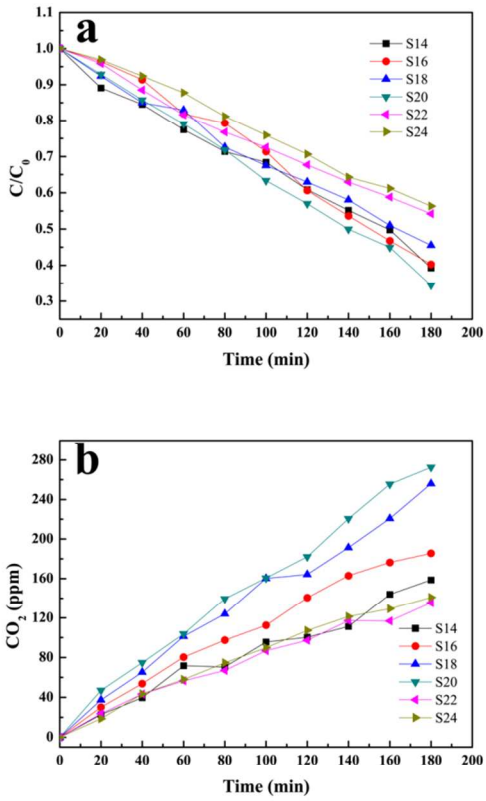

Fig. 4 Evaluation of the photocatalytic performance of the nanorod arrays: (a) by time course of the decrease in benzene concentration; (b) the increase of CO_2 concentration during photocatalysis.

keep decreasing with the decrease of the packing density. Whereas, the photocatalytic activity of the sample reaches the peak for sample S20, then it goes downwards with further increase of HCl usage. In other words, the sample S14 with the

CrystEngComm Accepted Manuscript

This journal is © The Royal Society of Chemistry 2012

most (002) facets exposed didn't demonstrate the great photocatalytic performance as expected. The explanation for this is that exposed facet is not the main factor related to photocatalytic activity in this research.

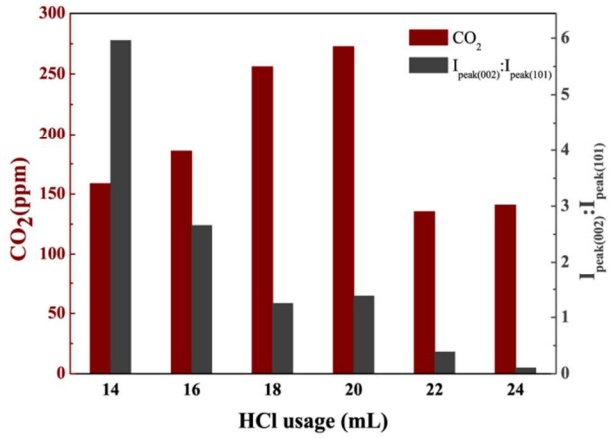

Fig. 5 The intensity ratio of the peak intensity between (002) and (101) facets, and the total CO_2 generated during the photocatalytic measurements.

Mechanism of the photocatalysis

Speaking of photocatalysis, the absorption of the incident light is a nonnegligible factor. It has been reported hierarchical structure can do benefits to light absorption.[26-30] As shown in the cross-section views of the nanorod film from Fig. 1, the packing density of the array significantly changed with the variation of HCl usage. This evidence gives a strong reason to speculate the influence of the film's morphology to light absorption. In order to understand the role that the film's morphology played during the light absorption, UV-Vis absorption measurement was investigated. Fig. 6 shows the UV-Vis absorption spectra in a wavelength range of 250 - 500 nm. All the samples demonstrate obvious absorption in the region of 250 - 400 nm. However, the absorption intensity of each sample is awfully different. Relatively sample S24 exhibits a poor absorption, which has the lowest packing density. As the increase of packing density, the absorption becomes elevated. They both reach the optimum point for sample S20. With further increase of packing density, the absorption turns to go downhill.

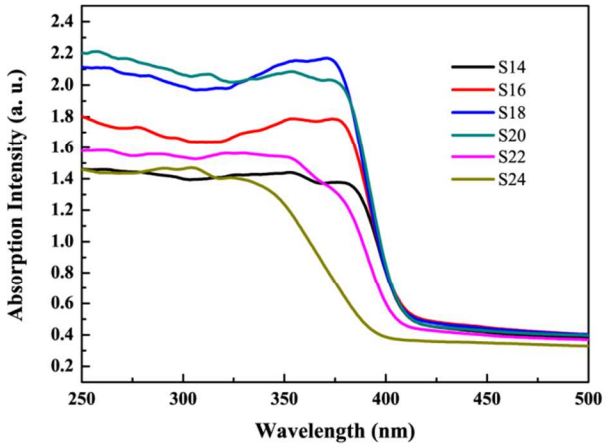

Fig. 6 UV-Vis absorption spectra of the nanorods films synthesized with different HCl usage.

Moreover, we calculated the average absorption of the film in the range of 250 – 400 nm. Fig. 7 lays out average absorption of each sample along with their total CO_2 generated during photocatalysis. As shown in the figure, it is obvious that the variation of the samples' average absorption has the same distribution corresponding to their photocatalytic performance. Sample S20 exhibits both best light absorption and photocatalytic activity. In other words, the ideal structure is obtained by using 20 mL HCl in the synthesis process. And it exhibited enhanced light absorption in the range of 250 – 400 nm, for which the photocatalytic performance is greatly promoted.

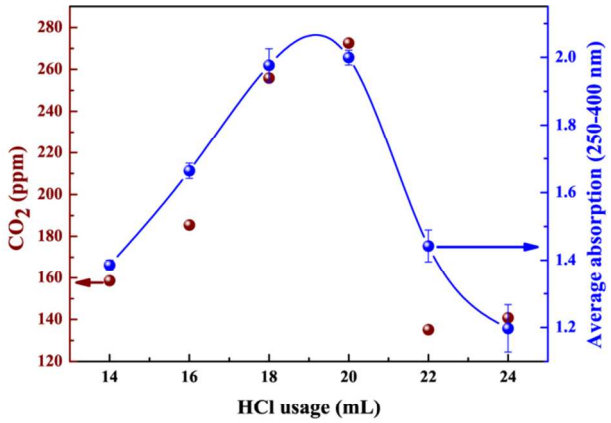

Fig. 7 The average absorption in the range of 250 – 400 nm for each sample, and the total amount of CO_2 generated during the photocatalytic measurements.

The explanation to this is that an appropriate packing density builds up an ideal array structure for light harvesting efficiency, due to the light trapping effect.[26-31] Fig. 8 illustrates this mechanism. Specifically, for loosely packed array, the incident light can be multi-reflected between the nanorods, promoting the absorption intensity of the film. Initially, this light trapping effect is not that obvious for sample S24 with an extremely low packing density. However, the light trapping effect gets more remarkable with the packing density going up such as S22 and S20. Judged by our results, the sample S20 has the most ideal packing density for the light trapping effect. When packing density keeps increasing, nanorods are more likely to run into neighboring rods, leaving no space for light to be multi-reflected between. It eliminates the light trapping effect.

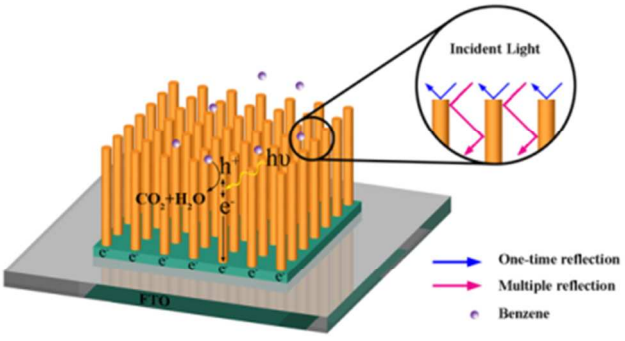

Fig. 8 Schematic diagram of light trapping effect for enhanced light harvest-

Based on the IPCE theory for photovoltaics, the IPCE equation is described as follows[32]:

$$\mathrm{IPCE}(\lambda) = \mathrm{LHE}(\lambda)\varphi_{\mathrm{inj}}(\lambda)\varphi_{\mathrm{reg}}(\lambda)\eta_{\mathrm{CC}}(\lambda) \quad (1)$$

CrystEngComm Accepted Manuscript

where LHE is the light harvesting efficiency, φ_{inj} and φ_{reg} are the quantum yields for electron injection and dye regeneration, respectively, and η_{CC} is the charge collection efficiency. This equation of IPCE not only covers the incident photon's conversion to electron, but also the light harvesting efficiency as well, which is a nonnegligible factor for our research. In this paper, each sample has the same φ_{inj} and φ_{reg} due to the absence of dye in our photocatalysts. While η_{CC} is the function of charge collection length L_c and photoactive layer's thickness d.[32] So for the films with the same size and thickness, η_{CC} can be deem as a constant, which is the situation for our research. Hence, that leaves LHE the most important factor. The correlation between LHE and light absorption is defined as follows[32]:

$$\mathrm{LHE} = 1 - 10^{-A} \quad (2)$$

where A is the absorbance of the film. When Eq (1) and Eq (2) are integrated, it is predictable that IPCE should have the same variation of the light absorption for all the samples.

To further confirm our hypothesis, the measurement of photocurrent was carried out. Fig. 9 lays out the result of the photocurrent test. As expected, a distinctive response was observed. From the figure, sample S14, S16 and S24 exhibited barely any response, compared to the rest samples. Corresponded to photocatalytic activity and UV-Vis absorption result, the photocurrent of sample S20 dwarfs all the others as well. As we known, higher photocurrent means higher separation efficiency for photo-generated electrons and

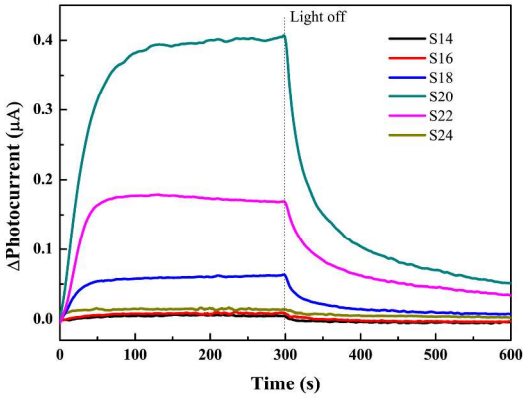

Fig.9 The response of the photocurrent test for the samples in air atmosphere.

holes, providing more long-lifetime charge carriers.[6] With more available electrons and holes, the photocatalytic activity can be promoted. Another reason for the decrease of photocurrent for sample S14 and S16 is that exorbitant packing density leads the nanorods bumping into each other. This brings more grain boundaries where the recombination of electrons and holes occurs.[33] Therefore, the photocatalytic activity drops down due to the decrease of the photo-generated charge carriers.

In conclusion, increasing packing density does provide more (002) facets, but meanwhile it results in that the nanorods become much closer to each other. Eventually when the nanorods merged into each other, it would erase the light trapping phenomenon and weaken the light harvesting efficiency, lessening photo-generated charge carriers. These are normally the disadvantages we try to avoid for photocatalytic materials. The optimum structure for photocatalysis was obtained by using 20 mL HCl with an enhanced light harvesting efficiency.

Conclusions

In summary, we introduced an ethanol-free hydrothermal method to fabricate TiO_2 nanorod array on FTO substrates with different packing density, by simply changing the volume ratio of hydrochloric acid and water. XRD and TEM confirmed the single crystallinity of the rutile TiO_2 nanorod with a high energy (002) facet exposed on top of the nanorod. To our surprise, the nanorod array packed with a higher density, meaning more (002) facets, didn't exhibit novel photocatalytic activity for decomposing gaseous benzene. However, the UV-Vis absorption and photocurrent measurement revealed that the light harvesting efficiency is the main factor for our work, due to the light trapping effect by the identical structure of the array. Combining all the results, it suggests that a medium arranged nanorod array has the optimum structure for photocatalysis with an enhanced light harvesting efficiency due to the light trapping effect, which is synthesized with 5 M HCl in the growth solution.

Acknowledgements

This work was supported by the National Basic Research Program of China (Grant Nos. 2009CB939705 and 2009CB939702). Also, the technology was supported by the Analytic Testing Center of HUST for carrying out XRD, FESEM, TEM and UV-Vis absorption analysis.

Notes and references

[a] State Key Laboratory of Materials and Processing Die & Mould Technology, Huazhong University of Science and Technology (HUST), No. 1037, Luoyu Road, Wuhan 430074, China
[b] Nanomaterials and Smart Sensors Research Laboratory, Department of Materials Science and Engineering, Huazhong University of Science and Technology, No. 1037, Luoyu Road, Wuhan 430074, China

1 H. N. Knudsen, U. D. Kjaer, P. A. Nielsen and P. Wolkoff, *Atmos. Environ.*, 1999, **33**, 1217.
2 R. Atkinson and J. Arey, *Chem. Rev.*, 2003, **103**, 4605.
3 J. G. Watson, J. C. Chow and E. M. Fujita, *Atmos. Environ.*, 2001, **35**, 1567.
4 K. R. Smith, J. M. Samet, I. Romieu and N. Bruce, *Thorax*, 2000, **55**, 518.
5 P. Wolkoff, *Atmos. Environ.*, 1998, **32**, 2659.
6 J.-M. Herrmann, *Appl. Catal. B,* 2010, **99**, 461.
7 A. Fujishima, X. Zhang and D. Tryk, *Surf. Sci. Rep.*, 2008, **63**, 515.
8 D. P. Macwan, P. N. Dave and S. Chaturvedi, *J. Mater. Sci.*, 2011, **46**, 3669.
9 K. Nakata and A. Fujishima, *J. Photochem. Photobiol. C,* 2012, **13**, 169.
10 K. Hashimoto, H. Irie and A. Fujishima, *Jpn. J. Appl. Phys.*, 2005, **44**, 8269.
11 B. Liu and E. S. Aydil, *J. Am. Chem. Soc.*, 2009, **131**, 3985.
12 H. Wang, Y. Bai, H. Zhang, Z. Zhang, J. Li and L. Guo, *J. Phys. Chem. C*, 2010, **114**, 16451.
13 Y. Li, M. Zhang, M. Guo and X. Wang, *Rare Met.* , 2010, **29**, 286.

CrystEngComm Accepted Manuscript

 This journal is © The Royal Society of Chemistry 2012

14 Y. Li, M. Guo, M. Zhang and X. Wang, *Mater. Res. Bull.* , 2009, **44**, 1232.
15 H. Yu, J. Pan, Y. Bai, X. Zong, X. Li and L. Wang, *Chem. Eur. J.*, 2013, **19**, 13569.
16 J.-S. Yang, W.-P. Liao and J.-J. Wu, *ACS Appl. Mat. Interfaces,* 2013, **5**, 7425.
17 X. Chen and S. S. Mao, *Chem. Rev.*, 2007, **107**, 2891.
18 M. Kong, Y. Li, X. Chen, T. Tian, P. Fang, F. Zheng and X. Zhao, *J. Am. Chem. Soc.*, 2011, **133**, 16414.
19 Y. Zhang, Y. Gao, X. H. Xia, Q. R. Deng, M. L. Guo, L. Wan and G. Shao, *Mater. Lett.*, 2010, **64**, 1614.
20 Q. Huang, G. Zhou, L. Fang, L. Hu and Z. Wang, *Energy Environ. Sci.*, 2011, **4**, 2145.
21 H. Li, C. Xie, Y. Liao, Y. Liu, Z. Zou and J. Wu, *J. Alloys Compd.*, 2013, **569**, 88.
22 B. J. Morgan and G. W. Watson, *J. Phys. Chem. C*, 2009, **113**, 7322.
23 R. S. Kavathekar, P. Dev, N. J. English and J. M. D. MacElroy, *Mol. Phys.*, 2011, **109**, 1649.
24 J. S. Chen and X. W. Lou, *Chem. Sci.*, 2011, **2**, 2219.
25 J. H. Lee and Y. S. Yang, *J. Eur. Ceram. Soc.*, 2005, **25**, 3573.
26 Y. S. Ding, X. F. Shen, S. Gomez, H. Luo, M. Aindow and S. L. Suib, *Adv. Funct. Mater.*, 2006, **16**, 549.
27 H. Sai, Y. Kanamori, K. Arafune, Y. Ohshita and M. Yamaguchi, *Prog. Photovolt. Res. Appl.*, 2007, **15**, 415.
28 B. Janthong, Y. Moriya, A. Hongsingthong, P. Sichanugrist and M. Konagai, *Sol. Energy Mater. Sol. Cells*, 2013, **119**, 209.
29 D. R. Rolison, J. W. Long, J. C. Lytle, A. E. Fischer, C. P. Rhodes, T. M. McEvoy, M. E. Bourg and A. M. Lubers, *Chem. Soc. Rev.*, 2009, **38**, 226.
30 O. Lupan, L. Chow, G. Chai, B. Roldan, A. Naitabdi, A. Schulte and H. Heinrich, *Mater. Sci. Eng. B*, 2007, **145**, 57.
31 J. Yang, W. Liao and J. Wu, *ACS Appl. Mater. Interfaces*, 2013, **5**, 7425.
32 A. Hagfeldt, G. Boschloo, L. Sun, L. Kloo and H. Pettersson, *Chem. Rev.*, 2010, **110**, 6595.
33 R. Leary and A. Westwood, *Carbon*, 2011, **49**, 741.

CrystEngComm Accepted Manuscript